EVACES2021
9th International Conference on Experimental Vibration Analysis for Civil Engineering Structures
14-17 September, 2021 ONLINE

Damage detection and localization using autocorrelation functions with spatiotemporal correlation

Jyrki Kullaa

Principal Lecturer, Department of Automotive and Mechanical Engineering, Metropolia University of Applied Sciences, Helsinki, Finland.

ABSTRACT

In vibration-based structural health monitoring, data analysis for damage detection can be done in the time domain or in the feature domain. Time-domain methods have certain advantages compared to feature-domain methods. For example, statistical analysis may be more reliable, because the data dimensionality is often low and the number of data points large. In addition, the algorithm can be fully automated, because system identification is not necessary. In this paper, autocorrelation functions (ACF) replace the direct response measurements in the time-domain data analysis. ACFs have many advantages compared to the actual time history records. Their accuracy can be controlled by choosing a proper measurement period. Spatiotemporal correlation between the ACFs can be utilized, because they have the same form as a free decay of the system for stationary random processes. This makes it possible to manage with a smaller number of sensors. In the proposed method, a spatiotemporal covariance matrix is estimated using the ACFs of the training data from the undamaged structure under different environmental or operational conditions. Using novelty detection techniques, an extreme value statistics control chart is designed to detect damage. The direction of the largest discrepancy between the training and test data is used to localize damage. A numerical experiment was performed by simulating vibration measurements of a bridge deck under stationary random excitation and variable environmental conditions. The excitation or environmental variables were not measured. Damage was a crack in a steel girder. ACFs outperformed both direct measurement data and virtual sensor data in damage detection. Damage localization was successful in all cases.

Keywords: Structural health monitoring, Damage detection, Autocorrelation function, Spatiotemporal correlation, Environmental or operational effects.

1. INTRODUCTION

Structural health monitoring (SHM) of large civil engineering structures has many challenges. First, the excitation is unknown and the vibration response is only measured. The objective is to track changes in the vibration characteristics of the structure. If the excitation is stationary, the modal parameters (natural frequencies, mode shape vectors, and damping) can be extracted using system identification techniques particularly developed for output-only data [1–3].

Second, damage detection depends heavily on the signal-to-noise ratio (SNR) of the data [4]. Therefore, noise reduction is important. System identification can be also considered a means to reduce noise, because it includes a lot of averaging. Another approach that is applied less frequently is data analysis directly in the time domain using the raw measurement data or the corresponding virtual sensor data [5]. The method works also for nonstationary processes provided the number of sensors is greater than the number of active modes. Then the sensor network is redundant and it is possible to predict a sensor's reading using the remaining sensors' data at the same time instant (spatial correlation). Virtual sensing results in reduction of measurement noise, which can significantly enhance detection performance [6].

Third, influences of environmental or operational variability on the dynamic characteristics of the structure often mask the effects of damage [7]. The normal variability must be included in the training data in order to distinguish between the environmental or operational effects and damage [8].

Time-domain and feature domain methods for damage detection were compared [9], and it was found that the features were more sensitive to damage than the actual or virtual sensor data. This was probably due to the fact that the features had a higher SNR than the sensor data. However, damage detection in the time domain has certain advantages compared to that in the feature domain. For example, the data dimensionality is often lower and the number of data points larger, which is advantageous in statistical analysis. Also, the algorithm can be fully automated, as system identification is not necessary.

In this paper, time-domain damage detection is applied to autocorrelation functions (ACF) instead of measured time records. For stationary random excitation, the ACFs have the same form as the free decay. The free decays can then be treated as time-domain data. The ACFs can be estimated automatically and their accuracy can be controlled with the measurement period T [10]. In addition, the free decay has a special mathematical expression for each mode allowing temporal correlation. More specifically, one can predict the ACF at any time lag from two data points of the ACF. The ACFs between sensors are also correlated making it possible to utilize spatiotemporal correlation. The number of time lags in the ACFs can be selected to control the amount of data. Training data under different environmental or operational conditions are nevertheless needed.

The paper is organized as follows. Autocorrelation functions are introduced in Section 2. Damage detection and localization in the time domain under varying environmental or operational conditions is outlined in Section 3. Detection and localization of an open crack in a bridge girder are studied in Section 4, in which a finite element model is used to generate vibration measurements under different environmental and operational conditions. Concluding remarks are given in Section 5.

2. AUTOCORRELATION FUNCTIONS

Damage detection in the time domain is investigated by replacing the actual response measurements with corresponding autocorrelation estimates. This can be justified for stationary random processes [10]. Correlation functions are also primary data in output-only modal identification, because they include all the necessary information about the dynamic characteristics of a linear structure [2]. Auto- and cross-correlation have also been utilized in damage detection by applying singular value decomposition to the empirical Hankel matrix [11].

The autocorrelation function (ACF) of a zero-mean sample time history record $x(t)$ is [10]:

$$R_{xx}(\tau) = E\left[x(t)x(t+\tau)\right] \tag{1}$$

where $E[\cdot]$ is the expectation operator. The ACF can be estimated with a direct method or by using FFT computations [10]. An FFT-based method with a single FFT-spectrum is used this study, because it is much faster when the measurement period is very long.

For a viscously damped SDOF system under white noise excitation with a constant power spectral density S_0, the displacement autocorrelation function at lag τ can be expressed as [12]:

$$R_{xx}(\tau) = \frac{\pi\omega_n S_0}{2k^2\zeta}\left(\cos\omega_d|\tau| + \frac{\zeta}{\sqrt{1-\zeta^2}}\sin\omega_d|\tau|\right)\exp(-\omega_n\zeta|\tau|) \tag{2}$$

where ω_n is the natural angular frequency, k is the spring constant, ζ is the damping ratio, and $\omega_d = \omega_n\sqrt{1-\zeta^2}$ is the damped natural angular frequency. It can be seen that the ACF is symmetric about $\tau = 0$. Therefore, only positive lags τ will be considered. Then, Eq. (2) has the following form.

$$R_{xx}(\tau) = \left(A\cos\omega_d\tau + B\sin\omega_d\tau\right)e^{-a\tau} \tag{3}$$

where A, B, a, and ω_d is are constants. Notice that Eq. (3) has the same form as the free vibration of a viscously damped SDOF system. This particular form is now studied. The same form applies also to velocity and acceleration ACFs.

Consider three different time lags, for which R_{xx} are available: τ, $\tau + p\Delta t$, and $\tau + q\Delta t$. where p and q are positive integers. It is now proved that any three data points from the ACF are linearly correlated, or redundant.

$$\begin{aligned} R_{xx}(\tau + p\Delta t) &= \left[A\cos\omega_d(\tau + p\Delta t) + B\sin\omega_d(\tau + p\Delta t)\right]e^{-a(\tau+p\Delta t)} \\ &= \left[\cos\omega_d\tau(A\cos p\Delta t + B\sin p\Delta t)e^{-ap\Delta t} + \sin\omega_d\tau(-A\sin p\Delta t + B\cos p\Delta t)e^{-ap\Delta t}\right]e^{-a\tau} \\ &= \left[C\cos\omega_d\tau + D\sin\omega_d\tau\right]e^{-a\tau} \end{aligned} \tag{4}$$

where

$$\begin{aligned} C &= (A\cos p\Delta t + B\sin p\Delta t)e^{-ap\Delta t} \\ D &= (-A\sin p\Delta t + B\cos p\Delta t)e^{-ap\Delta t} \end{aligned} \tag{5}$$

are constants. Similarly,

$$R_{xx}(\tau + q\Delta t) = \left[E\cos\omega_d\tau + F\sin\omega_d\tau\right]e^{-a\tau} \tag{6}$$

where

$$\begin{aligned} E &= (A\cos q\Delta t + B\sin q\Delta t)e^{-aq\Delta t} \\ F &= (-A\sin q\Delta t + B\cos q\Delta t)e^{-aq\Delta t} \end{aligned} \tag{7}$$

are constants. Next, if the three data points are linearly dependent, the following relationship applies.

$$R_{xx}(\tau) = bR_{xx}(\tau + p\Delta t) + cR_{xx}(\tau + q\Delta t) \tag{8}$$

Now it is shown that b and c are constants independent of τ. Substituting Eqs. (3), (4), and (6) into Eq. (8), yields

$$\left(A\cos\omega_d\tau + B\sin\omega_d\tau\right)e^{-a\tau} = b\left[C\cos\omega_d\tau + D\sin\omega_d\tau\right]e^{-a\tau} + c\left[E\cos\omega_d\tau + F\sin\omega_d\tau\right]e^{-a\tau} \tag{9}$$

or

$$(-A + bC + cE)\cos\omega_d\tau + (-B + bD + cF)\sin\omega_d\tau = 0 \tag{10}$$

Because the equation must be valid for any τ, the terms in the parentheses must be zero. They are written in the matrix form

$$\begin{bmatrix} C & E \\ D & F \end{bmatrix}\begin{Bmatrix} b \\ c \end{Bmatrix} = \begin{Bmatrix} A \\ B \end{Bmatrix} \tag{11}$$

Because the coefficient matrix and the right-hand side vector are constants, the regression coefficients are fixed for the given time lags. This means that for any τ, $R_{xx}(\tau)$ can be computed if the values at time lags $\tau + p\Delta t$, and $\tau + q\Delta t$ are available. This is the basis for temporal correlation in damage detection. Mathematically, if matrix **H** is constructed by adding time-shifted ACFs as rows, then rank(**H**) = 2.

Spatial correlation is considered next. Let us assume that in a MDOF system only one mode is active with a mode shape vector $\boldsymbol{\phi}$. Then the modal coordinate for the whole system is $q(t)$. The response vector is then $\mathbf{x}(t) = \boldsymbol{\phi}q(t)$. The autocorrelation function at DOF i is

$$R_{x_ix_i}(\tau) = E\left[x_i(t)x_i(t+\tau)\right] = E\left[\phi_i q(t)\phi_i q(t+\tau)\right] = \phi_i^2 E\left[q(t)q(t+\tau)\right] = \phi_i^2 R_{qq}(\tau), \quad 0 \le \tau \le T \tag{12}$$

The ACFs at different DOFs are all of the same except for the scaling factor ϕ_i^2. Therefore, there is also spatial correlation between the ACFs of each mode, which can be utilized in damage detection if the response is measured with a sensor network. If the number of active modes n is greater than one, the modal matrix is $\boldsymbol{\Phi} = [\boldsymbol{\phi}_1\ \boldsymbol{\phi}_2 \ldots \boldsymbol{\phi}_n]$ and the ACF of DOF i is

$$R_{x_ix_i}(\tau) = E\left[x_i(t)x_i(t+\tau)\right] = E\left[\sum_r \boldsymbol{\Phi}_{ir}q_r(t)\sum_s \boldsymbol{\Phi}_{is}q_s(t+\tau)\right] = E\left[\sum_r\sum_s \boldsymbol{\Phi}_{ir}\boldsymbol{\Phi}_{is}q_r(t)q_s(t+\tau)\right] \tag{13}$$

For lightly damped modes and well-separated modal frequencies, the modal amplitudes $q_r(t)$ and $q_s(t)$ are almost statistically independent for $r \neq s$ [12]. In that case, Eq. (13) is approximately

$$R_{x_ix_i}(\tau) \approx E\left[\sum_r \boldsymbol{\Phi}_{ir}^2 q_r(t)q_r(t+\tau)\right] = \sum_r \boldsymbol{\Phi}_{ir}^2 R_{q_rq_r}(\tau) \tag{14}$$

For closely-spaced modes, the cross-terms in Eq. (13) cannot be neglected. How this affects damage detection would require further investigation.

Data accuracy, or more specifically, the signal-to-noise ratio (SNR), is an important factor in detection. Therefore, high accuracy of the ACF estimates should be pursued for in the design of an SHM system. The error variance of the ACF is

inversely proportional to the record length T [10]. Therefore, T should be as large as possible. The error also depends on the frequency-damping product $\omega_n\zeta$, with a larger product resulting in a smaller error [13]. It was also shown that the ACF estimate has a considerable noise tail, which is independent of the actual system, and should be removed [13]. In this study, the number of lags in the ACFs was chosen to be 300. It was also shown that white noise increases the error of ACF at zero lag [10], but band-limited white noise would affect also the first few time lags [14]. In this paper, however, all lags from τ equal to 0 to 300 were retained.

3. DAMAGE DETECTION AND LOCALIZATION IN THE TIME DOMAIN

Damage detection is applied to the ACFs in the time domain treating the ACFs as if they were measured time histories. Comparison is also made using the actual response measurements or the corresponding virtual sensor data. First, the covariance matrix with a selected model order are estimated using training data from the undamaged structure under different environmental or operational conditions. Whitening transformation is applied to the covariance matrix [15]. This transformation is then fixed and applied to the test data resulting in the residual vector between the model and the new data. All residuals are subjected to principal component analysis (PCA). Retaining the first principal component scores of the residuals, the data dimensionality is decreased to one. An extreme value statistics [16] control chart [17] is then designed for the first PC scores of the residuals with appropriate control limits and subgroup size [5]. In this paper, the probability of false alarms equal to 0.001 is used.

Damage location is assumed to correspond to the direction of the first principal component of the residuals. The largest projection of the first PC on the sensor DOFs is assumed to reveal the sensor closest to damage.

4. NUMERICAL EXAMPLE

Numerical simulations were performed using a finite element model of a stiffened bridge deck (Fig. 1). The structure was 30 m long and 11 m wide. It had four longitudinal and three lateral stiffeners. The modelling was done using four-node discrete Kirchhoff quadrilateral shell elements with a diagonal mass matrix. The deck was made of concrete with a Young's modulus of E = 40 GPa (at temperature T = 0°C), Poisson ratio of ν = 0.15, density of ρ = 2500 kg/m^3, and thickness of 250 mm. The stiffeners were made of steel (E = 207 GPa, ν = 0.30, ρ = 7850 kg/m^3). The longitudinal stiffeners had a web with a thickness of t = 16 mm and a height of h = 1.4 m. The bottom flange had a thickness of t = 50 mm and a width of b = 700 mm. The lateral stiffeners were 1.4 m high and 30 mm thick plates.

The nodes of the bottom flanges were simply supported at both ends of the bridge. Longitudinal displacements were fixed only at one end of the bridge. The corners of the concrete deck were supported in the lateral and vertical directions.

Temperature had an effect on the stiffness of the concrete deck. It was assumed that temperature along the width was constant, but along the length it was linearly varying including a zero-mean Gaussian noise with a standard deviation of σ_T = 0.2°C in each row of elements. The ends of the bridge were at random temperatures between –20°C and +40°C. The relationship between the temperature and the Young's modulus was stepwise linear as shown in Fig. 2 left. There were thus an infinite number of possible distributions of the Young's modulus in the bridge deck. Different realizations of the distributions of the Young's modulus along the bridge are plotted in Fig. 2 right. The Young's modulus of each element was constant, determined using the temperature at the midpoint. Notice that the temperature or the Young's modulus were not measured, but they were considered latent variables.

Two independent random loads were applied at two nodes in the vertical direction, shown as green squares in Fig. 1. Because ambient excitation was assumed, steady state response was measured. For the steady state analysis, periodic pseudorandom excitations in the frequency range between 0 and 20 Hz with random amplitudes and phases were generated [18], and the analysis was performed in the frequency domain [12]. The excitation was not measured.

The response was computed with a modal superposition algorithm using the first 30 modes. The analysis period was over 43 minutes, or more precisely 2621.44 s, with a sampling frequency of 100 Hz. One measurement period then included 2^{18} = 262,144 samples from each sensor.

Vertical accelerations were measured at 28 points shown in Fig. 1. An equal amount of noise was added to the signals, so that the average signal-to-noise ratio was SNR = 30 dB.

The number of measurements was 136. The first 100 measurements were acquired from the undamaged structure under random environmental conditions. Damage was a crack in a steel girder, which was simulated by removing the contact between elements at selected nodes. The crack was located between sensors 10 and 11, but slightly closer to sensor 11. The damage location is plotted in red in Fig. 1. Six different crack configurations were modelled with an increasing severity by

removing the contact at 1–6 nodes. They are shown in the detailed plot in Fig. 1 indicating the order in which the nodes were separated. Only the last damage scenario reached to the edge of the flange. Each damage scenario was monitored with six measurements under random environmental and operational conditions. As a result, the last 36 measurements were from a damaged structure.

Fig. 3 shows the first seven natural frequencies in all 136 measurements. The variability due to environmental variation is clearly seen. The vertical line separates the data from the undamaged and damaged structure. It is difficult to visually observe damage from the variability of the natural frequencies.

The training data were the first 70 measurements. They were also used to design the control charts. The test data were the last 66 measurements, from which the last 36 were from the damaged structure.

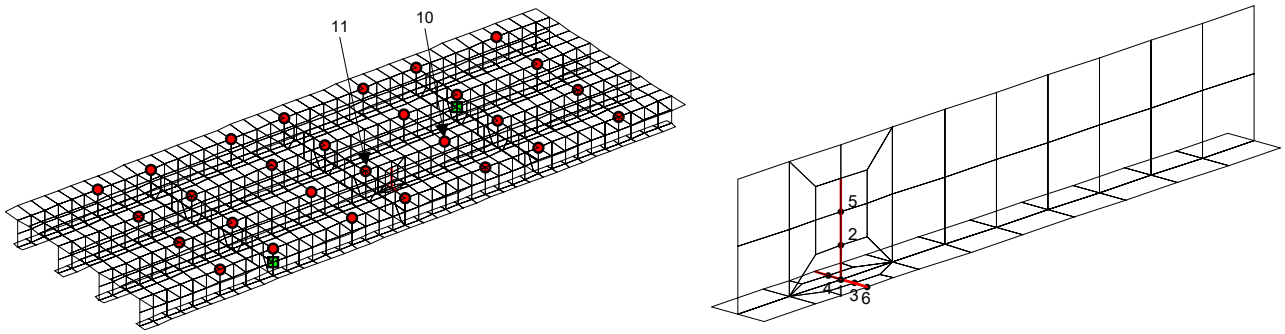

Figure 1. Left: Finite element model of a bridge deck. The 28 sensor positions are shown as red circles and the two excitation points as green squares. Damage is shown with red lines. Sensor 11 was located nearest to the crack. Right: A detail of the steel girder with damage. The crack is shown with red lines and the numbers indicate the order in which the connecting nodes separated resulting in an increasing crack size.

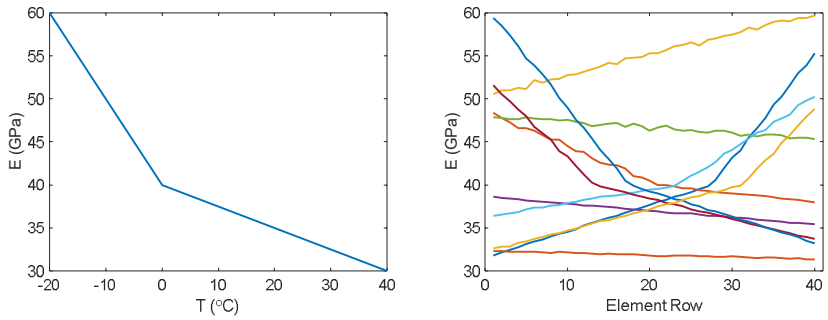

Figure 2. Left: The effect of temperature on the Young's modulus of the concrete. Right: Ten realizations of the longitudinal distributions of the Young's modulus of the concrete.

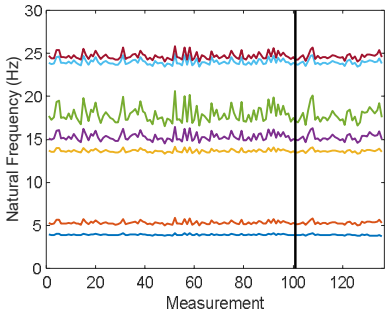

Figure 3. The first seven natural frequencies indicating the influences of the environmental variables and damage. The data on the left side of the vertical line were from the undamaged structure.

4.1. Time history analysis

For a reference, damage detection was performed analyzing both the physical and the virtual sensor data. Virtual sensors were estimated using the full time histories, but the first 1000 samples from each measurement were only selected for damage detection.

EVS control charts for damage detection are plotted in Fig. 4 with model order 0 for the physical sensor data (left) and virtual sensor data (right). The largest damage level was only detected from the physical sensor data, whereas the two largest damage levels were detected using the virtual sensor data. The same EVS control charts with model order 30 are shown in Fig. 5 for the physical sensor data (left) and virtual sensor data (right). The two largest damage levels were detected from the physical sensor data, whereas the three or four largest damage levels were detected using the virtual sensor data. Logarithmic scaling was applied to the vertical axes for clarity.

The advantageous effect of noise reduction of the virtual sensors on damage detection can be clearly seen. In addition, spatiotemporal correlation increased the detection performance with either data compared to spatial correlation only. In all cases, damage was localized to sensor 10.

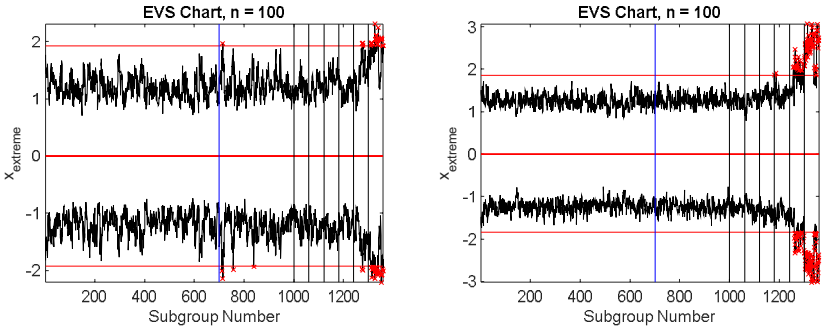

Figure 4. Damage detection using control charts with model order = 0. Left: Physical sensor data. Right: virtual sensor data. The data on the left side of the leftmost vertical line were used as the training data, and the other vertical lines indicate the six damage levels with an increasing severity.

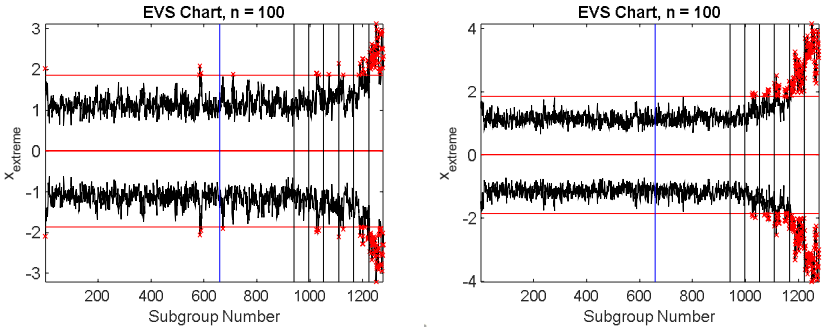

Figure 5. Damage detection using control charts with model order = 30. a) Physical sensor data, b) virtual sensor data.

4.2. Autocorrelation function analysis

The accuracy of the autocorrelation function depends on the measurement period T. Therefore, it is crucial to select a proper T. In this study, the number of samples was $N = 2^{18} = 262{,}144$ corresponding to $T = 44$ min. The autocorrelation functions at the first 300 lags were computed from a single FFT-spectrum. Model orders 0 and 30 were studied (spatial correlation and spatiotemporal correlation, respectively).

Sample autocorrelation functions from measurement 31 are shown in Fig. 6 left for all 28 sensors and on the right for sensors 9 and 25. Because the response included participation of several modes, the AFCs do not look like free decays of a single degree-of-freedom system.

The EVS control charts for the ACFs are plotted in Fig. 7 using spatial correlation only (left) or spatiotemporal correlation with a model order of 30 (right). With spatial correlation, damage level 1 remained undetected, while using spatiotemporal correlation, all damage levels were detected. Logarithmic scaling was applied to the vertical axis for clarity. With spatial

correlation, damage was localized to sensor 10 (Fig. 8 left), whereas using spatiotemporal correlation, damage was localized to sensor 11 (Fig. 8 right).

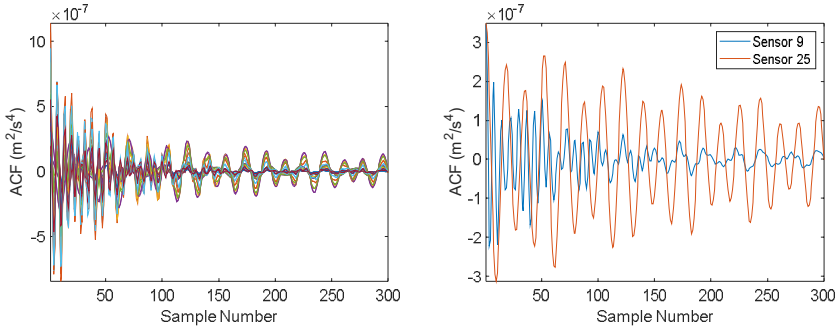

Figure 6. Estimated autocorrelation functions from measurement 31 with T = 44 min. Left: All 28 sensors. Right: Sensors 9 and 25.

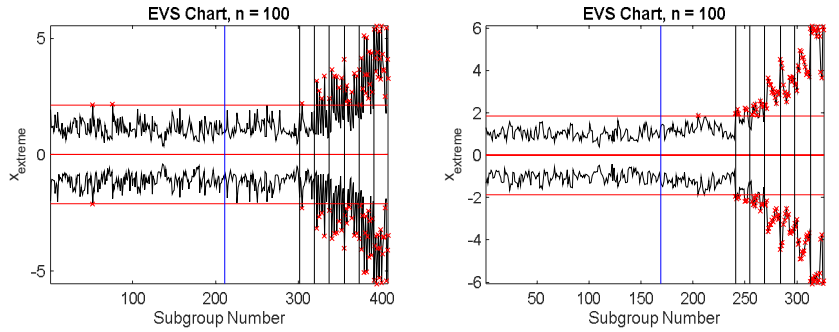

Figure 7. EVS control charts for ACFs with T = 44 min. Left: model order = 0. Right: model order = 30. The data on the left side of the leftmost vertical line were used as the training data, and the other vertical lines indicate the six damage levels with an increasing severity.

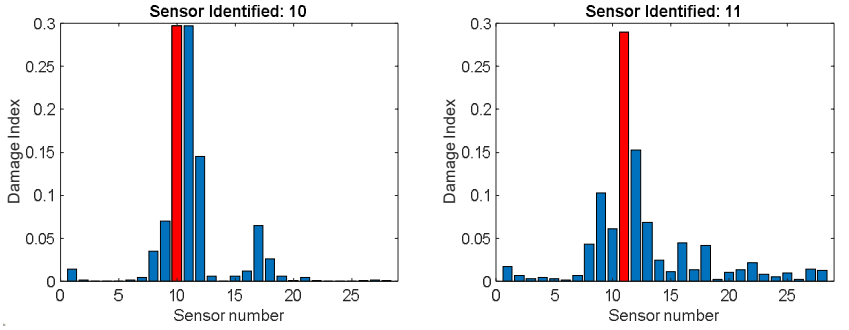

Figure 8. Damage localization using autocorrelation functions. T = 44 min. Left: model order = 0. Right: model order = 30.

5. CONCLUSIONS

Correlation functions play a key role in operational modal analysis. However, to the author's knowledge, this was the first time when autocorrelation functions were applied directly to damage detection in the time domain.

A comparison of damage detection performance was made using response time records or virtual sensor data. Because the measurement data and the detection algorithm were the same in all cases, differences in the results were due to the selected features only (physical sensor data, virtual sensor data, or ACFs). ACFs of a random process have a mathematical expression allowing spatiotemporal correlation to enhance detection. Moreover, the accuracy of the ACFs can be controlled by selecting a proper measurement period. In the simulated case, ACFs outperformed response data in damage detection provided a long measurement period was used. Spatiotemporal correlation produced better results than spatial correlation only. Damage localization was successful in all cases.

ACFs have also some limitations: the excitation is assumed stationary and the measurement period must be long. Fortunately, it is possible to use also shorter time records and estimate the spectral functions by averaging [10]. For nonstationary records, direct response data with model order equal to zero (spatial correlation) is an alternative.

Another issue are structures with damping depending on the vibration amplitude [3]. Then the temporal correlation is more complicated. A possible solution is to treat variable damping as an environmental influence, which must be present in the training data. This issue is left for a further study.

Another open question remains for structures with closely-spaced modes discussed in Section 2. The modal coordinates may be correlated, which has an influence on the ACFs and consequently on damage detection.

Other possibilities and limitations of ACFs in damage detection will be studied in the future. Experimental validation is also necessary.

ACKNOWLEDGEMENTS

This research has been supported by Metropolia University of Applied Sciences.

REFERENCES

[1] Brincker, R, Ventura, C. (2015). *Introduction to operational modal analysis.* Wiley, Chichester, West Sussex.
[2] Rainieri, C., Fabbroncio, G. (2014). *Operational modal analysis of civil engineering: An introduction and guide for applications.* Springer Science+Business, New York, USA.
[3] Au, S.-K. (2017). *Operational modal analysis. Modeling, Bayesian inference, uncertainty laws*. Springer, Singapore.
[4] Kay, S.M. (1998). *Fundamentals of statistical signal processing. Detection theory*. Prentice-Hall, Upper Saddle River, N.J., USA.
[5] Kullaa, J. (2020). "Robust damage detection in the time domain using Bayesian virtual sensing with noise reduction and environmental effect elimination capabilities." *Journal of Sound and Vibration*, 473, 115232.
[6] Kullaa, J. (2018). "Bayesian virtual sensing in structural dynamics." *Mechanical Systems and Signal Processing*, 115, 497–513.
[7] Sohn, H. (2007). "Effects of environmental and operational variability on structural health monitoring." *Philosophical Transactions of the Royal Society A: Mathematical, Physical and Engineering Sciences*, 365, 539–560.
[8] Kullaa, J. (2011). "Distinguishing between sensor fault, structural damage, and environmental or operational effects in structural health monitoring." *Mechanical Systems and Signal Processing* 25(8), 2976–2989.
[9] Kullaa, J. (2019). "Comparison of time domain and feature domain damage detection." *Proceedings of the 8th International Operational Modal Analysis Conference (IOMAC 2019)*, Copenhagen May 12–14, 2019, 115–126.
[10] Bendat, J.S., Piersol, A.G. (2010). *Random data: Analysis and measurement procedures*. 4th edition. Wiley, Blackwell, Hoboken, N.J., USA.
[11] Basseville, M. (2009). "Model-based statistical signal processing for change and damage detection." Encyclopedia of Structural Health Monitoring, Boller, C., Chang, F.-K., Fujino, Y. (eds.), Wiley, 677–695.
[12] Clough, R.W., Penzien, J. (1993). *Dynamics of structures.* 2nd edition. McGraw-Hill New York.
[13] Tarpø, M., Friis, T., Georgakis, C., Brincker, R. (2020). "The statistical errors in the estimated correlation function matrix for operational modal analysis." *Journal of Sound and Vibration*, 466, 115013.
[14] Orlowitz, E., Brandt, A. (2019). "Influence of noise in correlation function estimates for operational modal analysis." Mains, M., Dilworth, B.J. (eds.), *Topics in Modal Analysis & Testing, Volume 9, Conference Proceedings of the Society for Experimental Mechanics Series*, 55–64.
[15] Kullaa, J. (2012). "Whitening transformation in damage detection." Del Grosso, A.E., Basso P. (eds.), *Smart structures: Proceedings of the 5th European Conference on Structural Control — EACS 2012*, Genoa, Italy, June 18–20, 2012.
[16] Worden, K., Allen, D., Sohn, H. & Farrar, C.R. (2002). "Damage detection in mechanical structures using extreme value statistics." *SPIE Proceedings, Vol. 4693, 9th Annual International Symposium on Smart Structures and Materials*, San Diego, CA. 289–299.
[17] Montgomery, D.C. (1997). *Introduction to statistical quality control*, 3rd edition, Wiley, New York.
[18] Brandt, A. (2011). *Noise and vibration analysis: Signal analysis and experimental procedures.* Wiley, Chichester, Hoboken, N.J., USA.